JOURNAL OF AIRCRAFT
Vol. 44, No. 6, November–December 2007

Return from Airfoil Stall During Ramp-Down Pitching Motions

W. Sheng,* R. A. McD. Galbraith,† and F. N. Coton‡
University of Glasgow, Glasgow, Scotland G12 8QQ, United Kingdom

DOI: 10.2514/1.30554

This paper considers the unsteady reestablishment of fully attached flow of an airfoil from the stalled condition while undergoing ramp-down motions. The main purpose of the work was to extend the applicability of the Leishman–Beddoes dynamic-stall model during the return from stalled state to the low Mach and Reynolds numbers of the Glasgow unsteady database. This was done by the adoption of the Beddoes modeling philosophy and the technique of the lagging angle of attack that Sheng et al. ["A New Stall-Onset Criterion for Low Speed Dynamic-Stall," *Journal of Solar Energy Engineering*, Vol. 128, Nov. 2006, pp. 461–471; and "Improved Dynamic-Stall-Onset Criterion at Low Mach Numbers," *Journal of Aircraft* (to be published)] proposed for developing a new dynamic-stall onset criterion. It is concluded that a more secure assessment was obtained of the nondimensional time taken to convect the stalled flow over and away from the airfoil, compared with those of Niven et al. ("Analysis of Reattachment During Ramp Down Tests," *Vertica*, Vol. 13, No. 2, 1989, pp. 187–196) and Green and Galbraith ("Dynamic Recovery to Fully Attached Aerofoil Flow from Deep Stall," *AIAA Journal*, Vol. 33, No. 8, 1995, pp. 1433–1440). This, combined with the appropriate lift-curve slope, yielded an improved data reconstruction over that of the Leishman–Beddoes model. The present depiction and modeling of the reestablishment of fully attached flow from stalled state is a valid enhancement to the Leishman–Beddoes model.

Nomenclature

c	=	chord length, m
c_c	=	chordwise force coefficient
c_d	=	drag coefficient
$c_{N\min}$	=	normal force coefficient at its local minimum value during the downstroke motion of airfoils
c_n	=	normal force coefficient
$c_{n\alpha}$	=	best slope of the normal force coefficient
c_p	=	pressure coefficient
$\lvert c_p\rvert$-rise	=	pressure coefficient suction rise at the leading edge (normally 2.5% chord)
$dc_n/d\alpha$	=	downstroke slope of the normal force coefficient before full reattachment
f	=	separation location in terms of chord
f', f''	=	delayed separation function of f
M	=	Mach number
r	=	reduced pitch rate, $\dot{\alpha}c/2V$
s	=	nondimensional time, $2Vt/c$
s_1, s_2	=	coefficients for separation function representation
T_f	=	nondimensional time delay of the separation point due to dynamic effect
T_p	=	time-delay constant
T_r	=	nondimensional time-delay constant for the reattachment process
T_V	=	time constant of the vortex traveling over the chord
T_{VL}	=	vortex-passage-time constant
T_α	=	delay constant for the angle of attack due to dynamic effect
V	=	freestream velocity, m/s
V_x	=	shape function of the normal force due to the vortex
α	=	angle of attack or incidence, deg
$\alpha_{\rm cr}$	=	critical stall-onset angle of attack, deg
α_{ds}	=	stall-onset angle of attack, deg
α_{ds0}	=	constant critical stall-onset angle of attack, deg
$\alpha_{\min}$	=	angle of attack at $c_{N\min}$, deg
$\alpha_{\min 0}$	=	angle of attack at $c_{N\min}$ for the static test, deg
α_{ss}	=	static stall-onset angle of attack, deg
α_0	=	mean angle of attack in the oscillating motion of the airfoil, deg
α_1	=	breakpoint of separation
Δ	=	step change in forcing or in time
Δc_{mv}	=	pitching moment due to the vortex
Δc_{nv}	=	additional normal force due to the vortex
η_m	=	forcing for the circulatory pitching moment
η_n	=	forcing for the circulatory normal force
κ	=	reduced frequency $\omega c/2V$
λ_m	=	forcing for the noncirculatory pitching moment
λ_n	=	forcing for the noncirculatory normal force
τ	=	nondimensional time-delay constant for reattachment
τ_v	=	nondimensional time during the vortex passage

Presented as Paper 1075 at the 45th AIAA Aerospace Sciences Meeting and Exhibit, Reno, NV, 8–11 January 2007; received 19 February 2007; revision received 30 May 2007; accepted for publication 5 June 2007.

*Research Assistant, Department of Aerospace Engineering; wsheng@aero.gla.ac.uk.

†Professor, Department of Aerospace Engineering; r.a.m.galbraith@aero.gla.ac.uk.

‡Professor, Department of Aerospace Engineering; f.coton@aero.gla.ac.uk.

I. Introduction

AS IS well-documented [1–7], deep dynamic stall is characterized for oscillatory pitching motions by large hystereses. The computational simulations [7–9] or reconstructions [9–14] of such unsteady airfoil performance are both difficult and problematic. Figure 1 is illustrative of the problem and depicts the reconstruction of the cyclical c_n of the NACA 0012 airfoil undergoing dynamic stall using the Leishman–Beddoes (L–B) dynamic-stall (DS) model [14].

It may be observed that the reestablishment of the fully attached state is not predicted well. This is hardly surprising, because the model has been developed and refined for the data of Mach numbers greater than 0.3, whereas the experimental data used here have a Mach number of about 0.12.

The difficulty with oscillatory pitching motions is that it is often difficult to isolate the effects of the associated flow phenomena when they may be occurring simultaneously. It was for this reason that constant pitch-rate motions (i.e., ramps) were investigated by Westland Helicopters [15] and continued at Glasgow University [16] and at United Technologies Research Center by Lober and Carta [17], to isolate the detailed contributions of each flow state. The

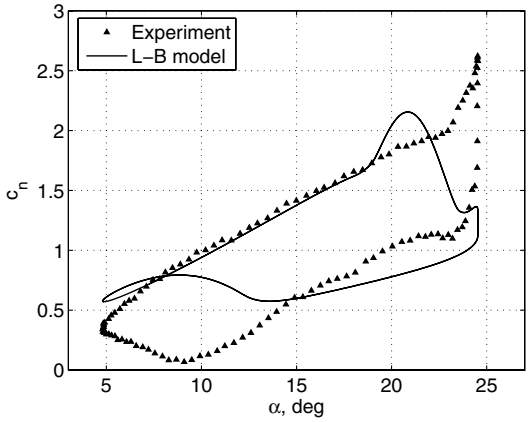

Fig. 1 Reconstruction of c_n by the L–B DS model, compared with experimental data (NACA 0102).

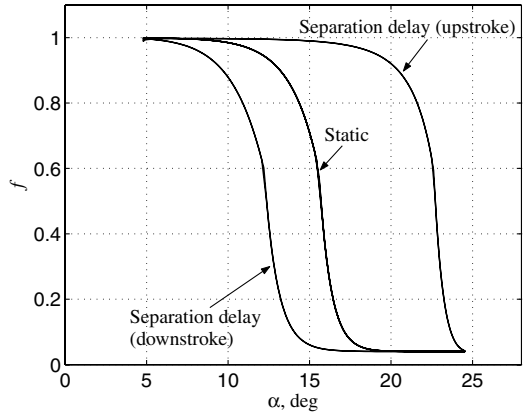

Fig. 2 Trailing-edge separation location of a static case and its lagged values of rapid upstroke and downstroke.

usefulness of the resultant measured unsteady pressure data of ramp-up tests was recently demonstrated by Sheng et al. [18,19] in the development of their new stall-onset criterion for low-speed dynamic stall. They further illustrated the new criterion's applicability to oscillatory pitching motions.

The underlying philosophy, indirectly expounded by Beddoes [20–23] and then by Leishman and Beddoes [14], was to attempt to model the extant physics, or flow descriptions, to at least a first order. In 1976, Beddoes [20] noticed that irrespective of the airfoil's reduced frequency, there were quite definite time constants that characterized the various parts of the aerodynamic hysteresis loop of c_n. This resulted in the Beddoes time-delay method [20], with the stall-onset criterion being that of a pitching-moment break correlation. As more detailed information became available, including "ramp" data, this model evolved and eventually became the popular L–B DS model [14].

Using this philosophy, and with detailed data for low-speed flows readily available, Niven et al. [24] developed a correlation for the initial phase of flow reattachment from stall. From that correlation, an enhancement to the model for the return from stall was initially developed. It included a time delay and a lift-curve slope associated with that part of the c_n curve. In that paper, however, no attempt was made to explain the reasons for the observations or, indeed, the seemingly anomalous data, in which there was a mix of ramp-rate-dependent and ramp-rate-independent data.

Green and Galbraith [25] eventually resolved the anomalous data by unraveling the two distinct events of the reattachment process that appear in the Glasgow data: 1) the "mush" of the stalled flow above the airfoil has to be convected over the upper surface before 2) the reestablishment of a fully attached boundary layer. The convection process was pitch-rate-independent, whereas the boundary-layer development was not. In other words, the mechanisms for the return

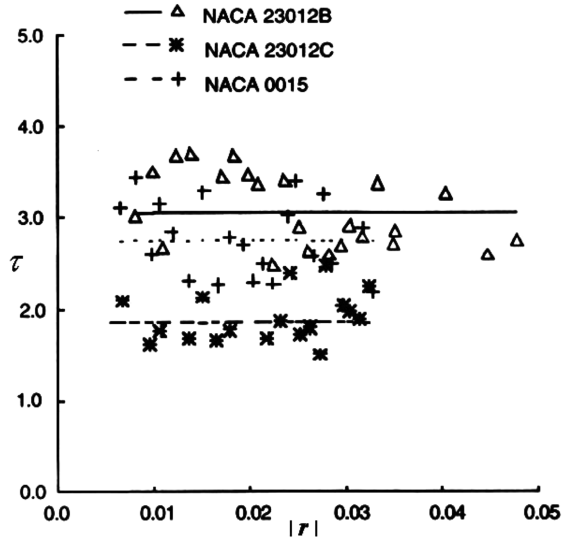

Fig. 3 Nondimensional time-delay constant for the reattachment process (Green et al. [26]).

from stalled state are similar: that is, a convective wave independent of pitch rate followed by a pitch-rate-dependent boundary-layer development. Depending on pitch rate, the processes may overlap each other. Similar processes are also found in [26–29].

The L–B DS model reconstructs the return from stall via a heavily lagged separation function proceeding from the leading edge to the trailing edge. Figure 2 illustrates a general progression of the separation location in such a model, including both upstroke and downstroke of a pitching motion. In Fig. 2, it may be seen that the lagging of the steady-state separation profile delays the movement of the separation point. An obvious lag in rapid pitch-down motion would significantly delay the achievement of fully attached flow.

By employing the Kirchhoff equation (1) and applying a separation point lagging, as depicted in Fig. 2, the L–B model can reconstruct the normal force with a hysteresis for an oscillatory airfoil (the reconstruction in Fig. 1). Unlike some of the measured data in ramp-down tests, however, this technique does not produce negative values of c_n at a significant positive incidence.

$$c_n = c_{n\alpha}(\alpha - \alpha_0)\left(\frac{1+\sqrt{f}}{2}\right)^2 \tag{1}$$

This methodology provided a distinct improvement to earlier modeling attempts but, at least for the low-speed cases, no longer reflected the processes involved in the return from stall. With the increased detailed ramp-down data available to Niven et al. [24], an attempt to model the return from stall for ramp-down motions was made simply by considering the c_n response. To do this, it was assumed that the rise of the magnitude of the pressure coefficient on the suction side at the 2.5% chord indicated the start of reestablishment of fully attached flow. The difference between this start point and the timing of $c_{N\min}$ was taken to be the duration of the convective wave (i.e., all the stalled flow had left the trailing edge). Whether this is the case is of secondary importance, because the two relatively distinct markers offered appropriate timing marks.

The resultant nondimensional times from start to finish were then calculated and plotted as shown in Fig. 3. The most obvious feature of this figure is, of course, the scatter, which is reminiscent of that obtained for the duration of deep-stall development [30] or the convection speed of the dynamic-stall vortex.

Sheng et al. [18,19] developed a new stall-onset criterion specifically for low-speed airfoils that was more secure and better defined than those based on the Evans–Mort correlation [31]. The present paper advances that work by treating the return from stalled state in a similar manner and therefore enhances the results of Niven et al. [24]. It will be shown that the new procedure for assessing the time delay associated with the convective wave greatly reduces the

Table 1 Airfoils tested at the University of Glasgow

No.	Airfoil	Thickness	Chord	Span
1	NACA 23012	12%	0.55 m	1.61 m
2	NACA 23012A	12%	0.55 m	1.61 m
3	NACA 23012B	12%	0.55 m	1.61 m
4	NACA 23012C	16%	0.55 m	1.61 m
5	NACA 0015	15%	0.55 m	1.61 m
6	NACA 0018	18%	0.55 m	1.61 m
7	NACA 0021	21%	0.55 m	1.61 m
8	NACA 0025	25%	0.55 m	1.61 m
9	NACA 0030	30%	0.55 m	1.61 m
10	NACA 0012	12%	0.55 m	1.61 m
11	NACA 0015	15%	0.275 m	1.61 m
12	AHAVAW	21%	0.55 m	1.61 m
13	GUVA10	18%	0.55 m	1.61 m
14	SSC-A09	9%	0.50 m	1.61 m
15	RAE9645	12%	0.50 m	2.40 m

scatter (shown in Fig. 3). And what's more, there is also no requirement to make an assessment of the initiation of the return from stall in the procedure, because this follows automatically from the methodology. Even when it is difficult to pinpoint the instant of $c_{N\min}$, an appropriate correlation may be still obtained, provided good data are available within a restricted range.

II. Glasgow Database

The Glasgow database of unsteady aerodynamic data contains information on the dynamic stalling of airfoils and wings and on blade–vortex interactions. Of relevance to the present work are those data associated with 2D dynamic stall. To date, fifteen 2D airfoils have been tested and these are listed in Table 1, together with the section profiles. All but one of the airfoils were mounted vertically in the Glasgow Handley–Page wind tunnel and pitched at the quarter-chord location. That facility has a 2.14×1.61 m working section, and with the normal model chord of 0.55 m (three exceptions), the tests were carried out at a Reynolds number of 1.5×10^6 and a Mach number of 0.12. Surface pressure data were obtained via miniature pressure transducers.

III. Modeling of the Reattachment Process

As mentioned previously, the enhancement to the L–B model considered here is simply that of an assessment of the convective part of the reattachment process (in particular, during the return from the fully stalled condition while undergoing ramp-down pitch displacements). Niven et al. [24] had taken the start of that process to be the suction pressure rise at the 2.5%-chord location. There was no particular significance about this location and it could have been taken anywhere in the leading-edge suction region. Nonetheless, some indication of the onset of the return from stall had to be chosen and 2.5% seemed, at that time, to be reasonable. The recovery in leading-edge suction ($|c_p|$-rise) may be observed in Fig. 4, which depicts the pressure coefficient against both time (Fig. 4a) and incidence (Fig. 4b).

In Fig. 4a, the evident fluctuations over much of the initial phase of the ramp-down are associated with the bluff-body flow and therefore with the Strouhal vortex shedding frequency. The suction recovery $|c_p|$-rise is clearly indicated in both Figs. 4a and 4b.

The timing mark chosen for the completion of the convective process, and that adopted in the present work, was when the normal force coefficient c_n achieved a local minimum value. This marker is depicted in Fig. 5. Once again, the apparent oscillations in the initial phase of the motion (Fig. 5a) are indicative of classical bluff-body flow.

For each of the ramp-down rates, Green and Galbraith [26] calculated the nondimensional time between the start and completion of the convective process. The time-delay constants for the NACA 23012B, NACA 23012C, and NACA 0015 airfoils were calculated and presented in Fig. 3, in which there is a significant scatter. That scatter is a consequence of the uncertainties in both $|c_p|$-rise and $c_{N\min}$ being compounded. The averaging of the values results in the nondimensional time constants of 3.0, 1.9, and 2.9 (see Green and Galbraith [26]).

Figure 6 shows typical results in which the incidence of $|c_p|$-rise and $c_{N\min}$ are plotted against the reduced pitch rate. The figure illustrates the constancy, to a first order, of the $|c_p|$-rise angle and the linearity of the $c_{N\min}$ variation with reduced pitch rate.

According to Niven et al. [24], the $|c_p|$-rise was observed to be independent of reduced pitch rate, to a first order, and close to the fully stalled incidence. Given this, it may be assumed that at a reduced pitch rate of zero, the onset of the return from stall coincides with the $c_{N\min}$ angle (i.e., the fully stalled angle). This assumption is acceptable for the NACA 0015 in Fig. 6. As mentioned before, the actual location of $|c_p|$-rise may vary from airfoil to airfoil. In Fig. 6, the incidence at the $|c_p|$-rise is a weak function of reduced pitch rate and may not be coincident with the static stall incidence at $r = 0$. This may be a consequence of accepting that the $|c_p|$-rise assessment was at an arbitrary location of 2.5% of the chord. Unless the $|c_p|$-rise location is known a priori and an appropriate transducer is located there, uncertainty will always be present.

Here, a new method is proposed. Let α_1 and α_2 represent the incidences of $c_{N\min}$ and the supposed actual $|c_p|$-rise (not 2.5%c, necessarily), respectively. The data are then represented by the following functions:

$$\begin{cases} \alpha_1 = \alpha_1' + \lambda_1 r \\ \alpha_2 = \alpha_2' + \lambda_2 r \end{cases} \tag{2}$$

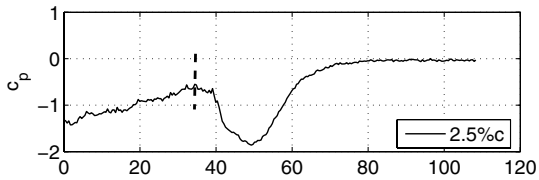

a) Nondimensional time, τ

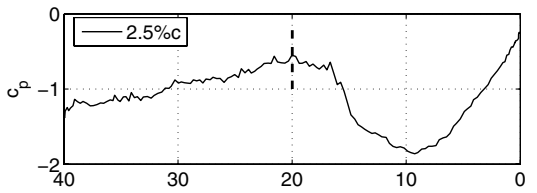

b) α, deg

Fig. 4 Pressure coefficient.

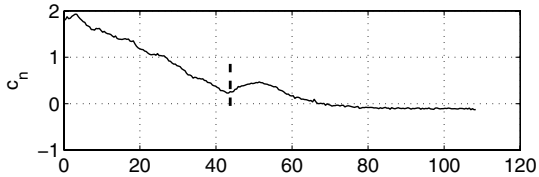

a) Nondimensional time, τ

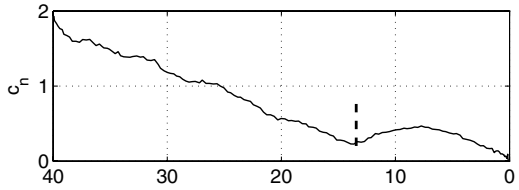

b) α, deg

Fig. 5 Normal force during a ramp-down test.

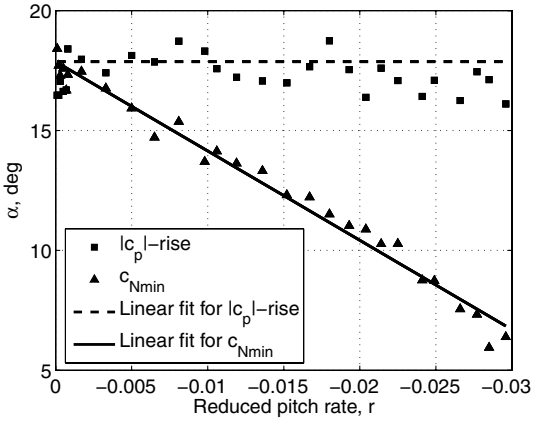

Fig. 6 Reattachment start ($|c_p|$-rise) and $c_{N\min}$ attained for NACA 0015.

For a particular reduced pitch rate, the difference $\Delta\alpha$ between α_1 and α_2 is

$$\Delta\alpha = (\alpha_1' - \alpha_2') + (\lambda_1 - \lambda_2)r \tag{3}$$

and the nondimensional time delay T_r can be calculated by

$$T_r = \frac{\alpha_1' - \alpha_2'}{r} + \lambda_1 - \lambda_2 \tag{4}$$

Because T_r is considered to be a constant, it must be independent of reduced pitch rate r, and so we have at $r = 0$

$$\alpha_1' - \alpha_2' = 0 \quad \text{or} \quad \alpha_1' = \alpha_2' \tag{5}$$

This is a perfectly reasonable simplification given that at $r = 0$ (i.e., steady flow) both α_1' and α_2' should coincide. Similar to the conclusion of Niven et al. [24], the $|c_p|$-rise (not 2.5%c, necessarily) was supposed to be virtually independent of r, then $\lambda_2 = 0$. Hence,

$$T_r = \lambda_1 \tag{6}$$

From the preceding analysis, only one linear fit (i.e., $\alpha_1 = \alpha_1' + \lambda_1 r$) is needed for the new proposed method, and it can be rewritten as

$$\alpha_{\min} = \alpha_{\min 0} + \lambda_1 r \tag{7}$$

A least-squares fit to the test data provides both $\alpha_{\min 0}$, and λ_1. From these, T_r can be obtained via Eq. (6). The values of $\alpha_{\min 0}$, T_r, and $dc_n/d\alpha$ for different airfoils are listed in Table 2.

Accordingly, the preceding analysis negates the requirement to make any assessment of the location of the $|c_p|$-rise at the leading edge of the airfoil. The onset of the return from the stall simply follows when the curve fit to the $c_{N\min}$ data crosses the y axis. Figure 7 is indicative of the obtained results.

The preceding methodology, therefore, provides both the required duration T_r of the convective phase and its implied onset angle $\alpha_{\min 0}$ of reattachment start. Together with the average gradient of the appropriate ramp-down normal force curve $dc_n/d\alpha$, this completes the required empirical inputs to the modification of Niven et al. [24] to the L–B model. As will be discussed, the $dc_n/d\alpha$ values could be different for ramp-down and oscillatory motions.

Table 2 Values of $\alpha_{\min 0}$, T_r, and $dc_n/d\alpha$ for different airfoils

Airfoil	$\alpha_{\min 0}$, deg	T_r	$dc_n/d\alpha$
NACA 0012	16.57	5.82	0.0589
NACA 0015	17.87	6.50	0.0556
NACA 0018	20.78	5.86	0.0550
NACA 23012	21.15	3.50	0.0539
NACA 23012A	21.45	5.42	0.0627
NACA 23012B	18.75	6.54	0.0468
NACA 23012C	23.24	5.07	0.0545
AHAVAW	21.29	5.06	0.0528
GUVA10	20.07	6.18	0.0506

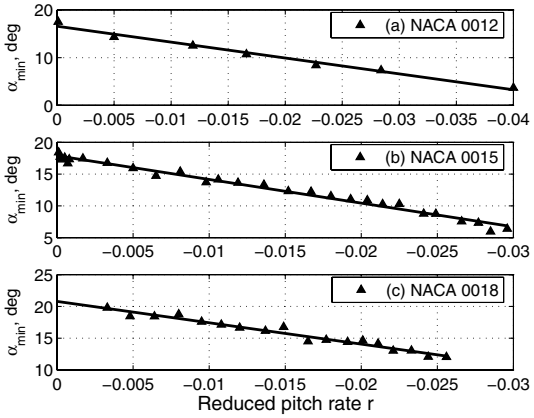

a) NACA 0012, NACA 0015, and NACA 0018

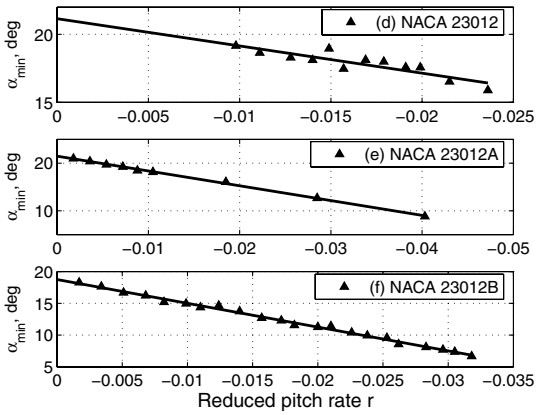

b) NACA 23012, NACA 23012A, and NACA 23012B

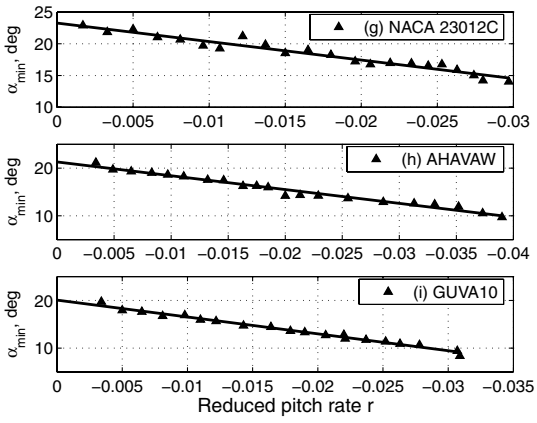

c) NACA 23012C, AHAVAW, and GUVA10

Fig. 7 Incidences at $c_{N\min}$ and the corresponding linear fits for different airfoils.

IV. Results and Discussion

The new model in this section incorporates the return modeling described in the previous section and the stall-onset criterion of Sheng et al. [18,19] into the original L–B DS model (see the appendices for details). For ramp-downs, the model is initiated from a measured c_n value at a fully stalled incidence. The reconstruction of c_n then follows the measured c_n slope value until the incidence is reduced to $\alpha_{\min 0}$, then the calculation proceeds continuously until the time delay T_r is expired when the convective phase is assumed to be

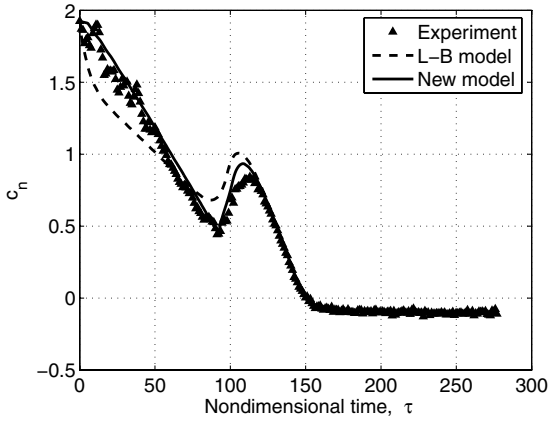

a) r = -0.005

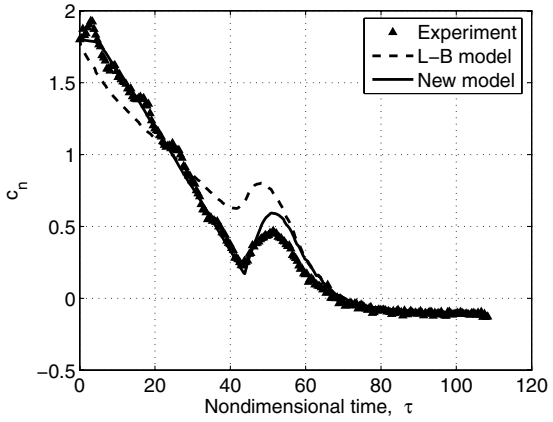

b) r = -0.0119

Fig. 8 Normal force reconstructions of ramp-down tests for NACA 0015.

complete. After that, an exponential return to the fully attached state is implemented to facilitate a smooth return to the original L–B DS model and to simplistically mimic the reestablishment of a fully attached boundary layer.

Figure 8 is representative of the ability of the model to reconstruct the measured data for ramp-down tests from the fully stalled condition to the fully attached condition. Results from the original L–B DS model are also compared with the measured data for the NACA 0015 airfoil.

In Fig. 8a, which shows low pitch-rate cases, the reconstruction of c_n is in excellent agreement with the measured data, better than that of the L–B model. This is because the L–B model considers the boundary-layer reestablishment only and does not include the convective phase of the process. The reduced pitch rate in Fig. 8b is much higher than that in Fig. 8a, and the current modeling procedure may be seen to be a significant improvement over the original L–B model. In this case, however, the exponential return to the original model has significantly overpredicted the measured data. Although this is of concern, the return to the original model does not form the thrust of the present work, which was simply to model the convective phase; for this, it does rather well.

As stated previously, ramp-type data were used in the development of the current technique to minimize any conflict of timing between the various phases of the dynamic stalling process found in oscillatory motions. For the current model, which reconstructs, to a good accuracy, the convective phase of the reattachment process during ramp-downs, it also must be applied to the oscillatory motions if it is to be of any long-term value.

Figure 9 presents a typical result for an oscillatory case, in which it may be observed that, using the normal force curve slope obtained from the ramp-down motions, the gradient is far too shallow when compared with the measured data in an oscillatory motion. The

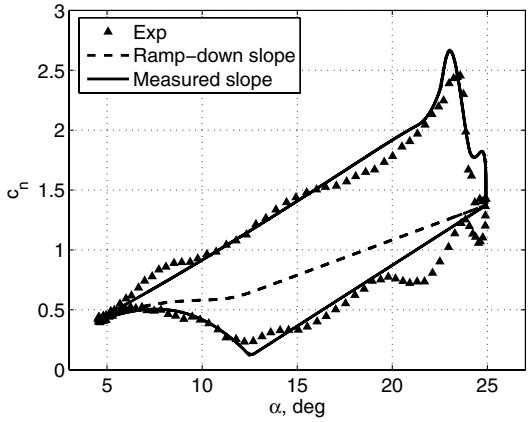

Fig. 9 Normal force reconstructions with different slopes during downstroke for NACA 0012 ($\kappa = 0.075$).

important point to note, however, is that albeit the gradient is low, the duration of the convective phase is well-predicted.

For a ramp-down test at the University of Glasgow, the testing sequence was that, previous to the data recording, the airfoil was continuously pitched up to the start angle of the ramp-down from a low angle of attack and held there for about 4 s seconds (approximately 160 chord lengths of travel). Then the airfoil linearly ramped down to low incidence again. From the sequence, we can see that just before the initiation of the ramp-down, the airfoil behaves as a bluff body with periodic vortex shedding. This shedding induces small changes in the effective incidence of the airfoil that are manifest as unsteadiness in the recorded normal force. In essence, however, the flow could otherwise be considered to be steady, with the near wake of the airfoil having no significant vortical content. Conversely, in an oscillatory test, vorticity is continually shed into the near wake of the airfoil as the lift changes due to the pitching motion. This implies that just before the downstroke, the wake of the airfoil will be populated by vorticity shed during the upstroke. Also, just before the downstroke, there is a rapid drop in normal force that will result in concentrated vorticity being shed into the airfoil wake. The sense of this vorticity will be to increase the effective incidence of the airfoil at the start of the convective phase. As this vorticity convects downstream, its influence will diminish. The net effect will be to steepen the normal force curve during the convective phase.

Careful inspection has revealed that for the oscillatory motions in which stall occurs, the c_n gradient, during the convective phase, is close to that of the fully attached flow portion of the model upstroke. Accordingly, that gradient was adopted and is readily available, either from the measured data or the model predictions. Using this gradient, the result is as indicated in Fig. 9. There it may be observed that not only is the reconstruction of the data improved but, most important, the concept of a convective wave does indeed work well.

There are, however, additional modeling considerations that could receive attention. In particular, there are clearly secondary vortices generated and convected away during the return from stall. The current modeling does not include these.

Figures 10 and 11 present the results of c_n during oscillatory motions. The new model produces a significant improvement compared with the original model. For the purposes of a fairer comparison, however, an additional prediction is also included when the original L–B model incorporates the stall-onset criterion of Sheng et al [18,19] [referred to as "L–B model (mod)" in Figs. 10 and 11]. Hence, the upstrokes appear to be identical and so produce a proper comparison for the return from stall.

Perhaps the most striking feature of these figures is the ineffectiveness of the L–B model to reconstruct the c_n response on the downstroke. It appears that the recognition of the two distinct phases of the return from stall in the current method has yielded an improved reconstruction, compared with the measured data.

Despite this, two important areas still require careful consideration if higher-fidelity modeling is to be achieved: first, the interaction of the vortex shedding and the convection of the stalled flow from the

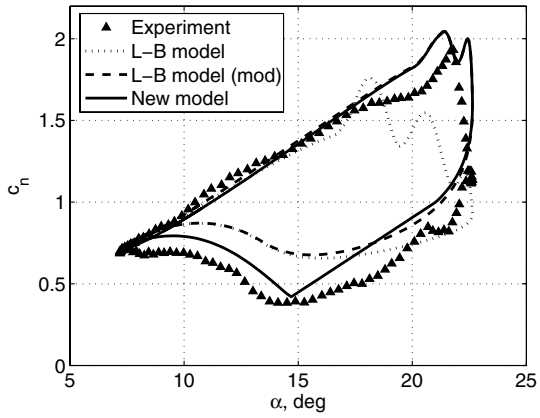

a) $\kappa = 0.078$

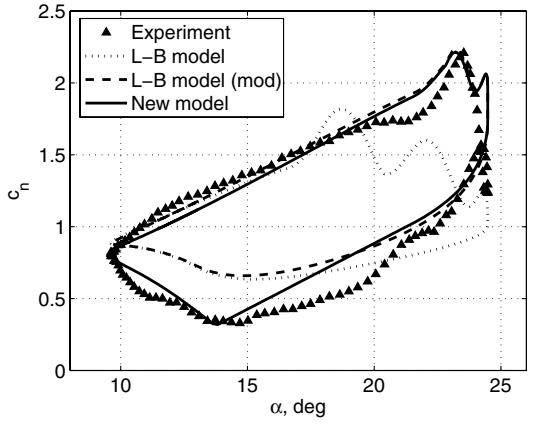

b) $\kappa = 0.102$

Fig. 10 c_n reconstructions of oscillatory tests for NACA 0015.

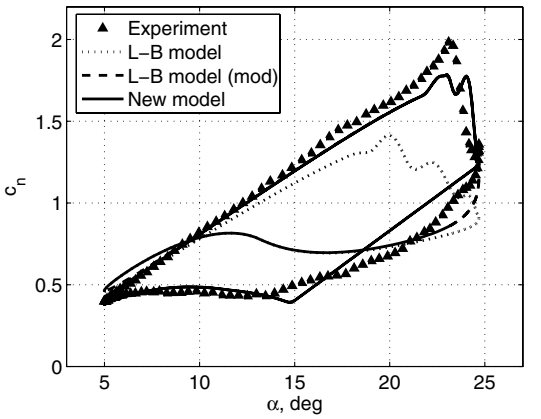

a) $\kappa = 0.076$

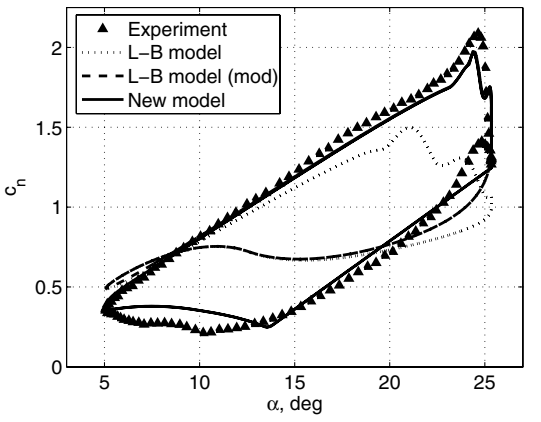

b) $\kappa = 0.101$

Fig. 11 c_n reconstructions of oscillatory tests for NACA 23012B.

upper surface during oscillatory pitching motions, and second, the interaction of the reestablishment of the attached boundary layer with the convection phase of the process. These will be the subject of future work.

V. Conclusions

1) A new method of modeling the unsteady establishment of fully attached flow during pitch-down motions was proposed. The method is based on the observation that the reestablishment process can be split into two phases: a convective phase and a reduced pitch-rate-dependent phase associated with the reestablishment of the boundary layer.

2) By considering the local minimum value $c_{N\min}$ of normal force during a ramp-down over a range of the reduced ramp rates, the acquisition of both the onset angle of the convective phase and its duration may be assessed.

3) The onset angle $\alpha_{\min 0}$ and duration of the convective phase T_r, together with the normal force curve slope $dc_n/d\alpha$ in the fully stalled region, provides the three empirical inputs to the L–B DS model.

4) The modeling procedure reduced the scatter associated with the methodology used by Niven et al. [24].

5) By observation, the required value of $dc_n/d\alpha$ during the convective phase in oscillatory motions is better represented by measured slope, normally paralleling to the fully attached portion of upstroke.

6) The present model displays a significant improvement for the predictions of ramp-down and oscillatory motions over the L–B DS model.

All of the preceding are related solely to low-speed flow and, in particular, to a Reynolds number in the region of 1.5×10^6 and an associated Mach number of 0.12.

Appendix A: Leishman–Beddoes Model

I. Airloads for Attached Flow

Circulatory components:

$$\Delta c_n^c(s) = c_{N\alpha}\Delta\eta_n(1 - A_1 e^{-b_1 s} - A_2 e^{-b_2 s} - A_3 e^{-b_3 s}) \tag{A1a}$$

$$\Delta c_m^c(s) = \Delta\eta_m \frac{\pi}{4\sqrt{1-M^2}}(1 - e^{-s/T_M}) \tag{A1b}$$

Impulsive components:

$$\Delta c_n^I(s) = \Delta\lambda_n \frac{4}{M} e^{-s/T_I} \tag{A1c}$$

$$\Delta c_m^I(s) = -\Delta\lambda_m \frac{4}{M} e^{-s/T_I} \tag{A1d}$$

with the forcing representations for a pure pitching motion at its quarter-chord axis

$$\begin{cases} \eta_n = \alpha + \frac{c}{2V}\dot{\alpha} \\ \eta_m = \frac{c}{2V}\dot{\alpha} \\ \lambda_n = \alpha + \frac{c}{4V}\dot{\alpha} \\ \lambda_m = \frac{1}{2}\alpha + \frac{7c}{24V}\dot{\alpha} \end{cases} \tag{A2}$$

and the coefficients

$$A_1 = 0.165, \quad A_2 = 0.335, \quad A_3 = 0.5 \quad b_1 = 0.05,$$
$$b_2 = 0.222, \quad b_3 = 0.8/M \quad T_M = M/2, \quad T_I = \frac{M(1+3M)}{2}$$

II. Airloads for Separated Flow

For a static test, Leishman and Beddoes [14] employed the Kirchhoff equation to calculate the normal force including separated flow:

$$c_n = c_{n\alpha}(\alpha - \alpha_0)\left(\frac{1+\sqrt{f}}{2}\right)^2 \tag{A3}$$

Therefore, the trailing-edge separation function f can be represented by piecewise exponential functions:

$$\begin{cases} f(\alpha) = 1 - 0.4\exp\left(\frac{\alpha-\alpha_1}{s_1}\right), & \alpha \le \alpha_1 \\ f(\alpha) = 0.02 + 0.58\exp\left(\frac{\alpha_1-\alpha}{s_2}\right), & \alpha > \alpha_1 \end{cases} \tag{A4}$$

Because of the induced camber effect under dynamic condition, a positive pitch rate decreases the leading-edge pressure for a given value of normal force. A T_p lagging to the unsteady normal force can stand for this effect as follows:

$$\Delta c_n'(s) = \Delta[c_n^c(s) + c_n^I(s)](1 - e^{-\frac{s}{T_p}}) \tag{A5}$$

From the comparison of the lagged normal force (A5) with the static normal force, an approximate T_p could be obtained (see Fig. A1, in which c_p is the pressure coefficient at 2.5%c).

Then an effective angle of attack is defined by the lagged normal force:

$$\alpha_{\text{eff}}(s) = \frac{c_n'(s)}{c_{n\alpha}} \tag{A6}$$

Based on the effective angle of attack, a delayed trailing-edge separation can be obtained:

$$\begin{cases} f'(\alpha) = 1 - 0.4\exp\left(\frac{\alpha_{\text{eff}}-\alpha_1}{s_1}\right), & \alpha' \le \alpha_1 \\ f'(\alpha) = 0.02 + 0.58\exp\left(\frac{\alpha_1-\alpha_{\text{eff}}}{s_2}\right), & \alpha' > \alpha_1 \end{cases} \tag{A7}$$

The unsteady airloads excluding dynamic stall can be assessed as the following forms:

$$c_n = (c_n^c + c_n^I)\left(\frac{1+\sqrt{f'}}{2}\right)^2 - c_{n\alpha} \times \alpha_0 \tag{A8a}$$

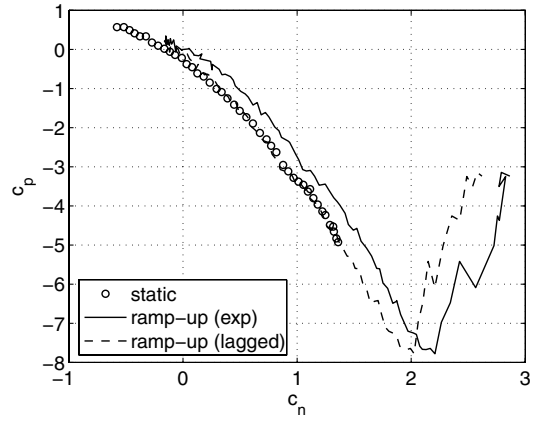

Fig. A1 Lagged normal force for a ramp-up test, compared with static normal force.

$$\frac{c_m - c_{m0}}{c_n} = k_0 + k_1(1 - f') + k_2\sin(\pi f'^2) \tag{A8b}$$

$$c_c = \eta c_{N\alpha}(\alpha - \alpha_0)^2\sqrt{f'} \tag{A8c}$$

$$c_d = c_{d0} + c_n\sin\alpha - c_c\cos\alpha \tag{A8d}$$

III. Dynamic-Stall Onset

Dynamic stall occurs when

$$c_n'(s) \ge c_{n1} \tag{A9}$$

with the critical normal force c_{n1} obtained from the static normal force that corresponds to either the break in the pitching moment or the chordwise force at stall (Leishman and Beddoes [14])

IV. Airloads Because of Dynamic Vortex

The modeling strategies for the airloads due to the dynamic vortex are outlined as follows:

1) The vortex forms at and detaches from the leading-edge region, inducing an overshoot in normal force as if the flow is still attached to the upper surface. Hence, its effect could be represented by a further boundary separation location delay:

$$\Delta f''(s) = \Delta f'(s)(1 - e^{-\frac{s}{T_f}}) \tag{A10}$$

2) At low Mach numbers, an additional overshoot in normal force occurs due to the vortex growing in strength and convecting across the chord. The additional normal force strength is believed to be proportional to the difference between the delayed separation location and its corresponding value in the steady case:

$$V_x = \sin^{3/2}\left(\frac{\pi\tau}{2T_V}\right) \quad \text{for } 0 < \tau < T_V \tag{A11a}$$

and, subsequently,

$$V_x = \cos^2\left[\frac{\pi(\tau - T_V)}{T_{VL}}\right] \quad \text{for } \tau > T_V \tag{A11b}$$

The additional overshoot due to the dynamic vortex is calculated by

$$\Delta c_{nv} = B_1[f'' - f] \times V_x \tag{A12}$$

3) The large nose-down pitching moment is induced due to the vortex convection over the chord. Its strength is proportional to the vortex normal force:

$$\Delta c_{mv} = B_2\left[1 - \cos\left(\frac{\pi\tau_v}{T_V}\right)\right] \times \Delta c_{nv} \tag{A13}$$

with the coefficients B_1 and B_2 adjustable for different airfoils.

V. Return from Stalled State

Leishman and Beddoes [14] suggested that the elements of the model are physically coupled. Hence, it is necessary to half or double the time constants during different dynamic stages. In our cases of low Mach numbers, the large hysteresis loop in normal force, especially the deep lagged return from the stalled state, suggests that doubling or quadrupling T_f is advisable for the reattachment stage.

Appendix B: Dynamic-Stall-Onset Criterion of Sheng et al.

Sheng et al. [18,19] employed a mathematical deduction and the correlation of measured data to develop a new dynamic-stall-onset criterion.

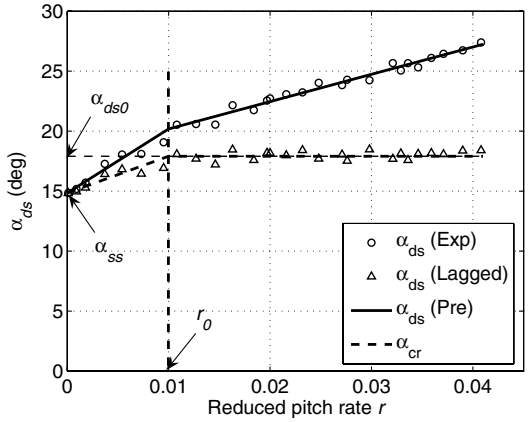

Fig. B1 A schematic graph for the new stall-onset criterion (Sheng et al. [19]).

First, a linear function for the relationship is employed to fit the stall-onset angle for reduced pitch rates larger than r_0; that is,

$$\alpha_{ds} = \alpha_{ds0} + m_1 r \tag{B1}$$

Equation (B1) was fitted to ramp-up test data (circles in Fig. B1) by a least-squares method, and the constants α_{ds0} and m_1 were obtained.

Second, a nondimensional time-delay constant was calculated by

$$T_\alpha = m_1 \tag{B2}$$

Third, a critical stall-onset angle is defined by

$$\begin{cases} \alpha_{\rm cr} = \alpha_{ds0}, & r \geq r_0 \\ \alpha_{\rm cr} = \alpha_{ss} + (\alpha_{ds0} - \alpha_{ss})\frac{r}{r_0}, & r < r_0 \end{cases} \tag{B3}$$

Lagging the angle of attack via the time constant T_α,

$$\Delta\alpha'(s) = \Delta\alpha(s)(1 - e^{-\frac{s}{T_\alpha}}) \tag{B4}$$

Finally, stall onset is said to occur when

$$\alpha' \geq \alpha_{\rm cr} \tag{B5}$$

To apply the new stall-onset criterion, the delayed trailing-edge separation function is obtained by referring the lagged angle of attack to the effective angle of attack, together with a angle of shift $\Delta\alpha_1$:

$$\begin{cases} \Delta\alpha_1 = \alpha_{ds0} - \alpha_{ss}, & r \geq r_0 \\ \Delta\alpha_1 = (\alpha_{ds0} - \alpha_{ss})\frac{r}{r_0}, & r < r_0 \end{cases} \tag{B6}$$

The new delayed separation function f' is now

$$\begin{cases} f'(\alpha) = 1 - 0.4\exp\left(\frac{\alpha' - \alpha_1 - \Delta\alpha_1}{s_1}\right), & \alpha' \leq \alpha_1 \\ f'(\alpha) = 0.02 + 0.58\exp\left(\frac{\alpha_1 + \Delta\alpha_1 - \alpha'}{s_2}\right), & \alpha' > \alpha_1 \end{cases} \tag{B7}$$

To replace the stall-onset criterion (A9) and the delayed trailing-edge separation function (A7) in the L–B model with the new stall-onset criteria (B3–B5) and the delayed trailing-edge separation function (B7), respectively, an initially modified L–B model is obtained ["L–B model (mod)" in Figs. 10 and 11]. The implementation of the return modeling proposed in this paper in the modified L–B model has finally resulted in a new model ("new model" in Figs. 10 and 11).

Acknowledgments

This research work is sponsored by the British Engineering and Physical Sciences Research Council (EPSRC), research grant no. GR/S42446/01 in collaboration with Garrad Hassan, Ltd. and the National Renewable Energy Laboratory's National Wind Turbine Center in Colorado.

References

[1] McAlister, K. W., Carr, L. W., and McCroskey, W. J., "Dynamic Stall Experiments on the NACA 0012 Airfoil," NASA TP 1100, 1978.

[2] McCroskey, W. J., Carr, L. W., and McAlister, K. W., "Dynamic Stall Experiments on Oscillating Airfoils," *AIAA Journal*, Vol. 14, No. 1, 1976, pp. 57–63.

[3] McCroskey, W. J., McAlister, K. W., Carr, L. W., Pucci, S. L., Lambert, O., and Indergrand, R. F., "Dynamic Stall on Advanced Airfoil Sections," *Journal of the American Helicopter Society*, Vol. 26, July 1981, pp. 40–50.

[4] Lee, T., Gerontakos, P., "Investigation of Flow over an Oscillating Airfoil," *Journal of Fluid Mechanics*, Vol. 512, July 2004, 313–341.

[5] Carr, L. W., "Progress in Analysis and Prediction of Dynamic Stall," *Journal of Aircraft*, Vol. 25, No. 1, 1988, pp. 6–17.

[6] Leishman, J. G., *Principles of Helicopter Aerodynamics*, Cambridge Univ. Press, New York, 2000.

[7] Carr, L. W., and Chandrasekhara, M. S., "Compressibility Effects on Dynamic Stall," *Progress in Aerospace Sciences*, Vol. 32, No. 6, 1996, pp. 523–573. doi:10.1016/0376-0421(95)00009-7

[8] Ekaterinaris, J. A., and Platzer, M. F., "Computational Prediction of Airfoil Dynamic Stall," *Progress in Aerospace Sciences*, Vol. 33, Nos. 11–12, 1998, pp. 759–846. doi:10.1016/S0376-0421(97)00012-2

[9] Spentzos, A., Barakos, G. N., Badcock, K. J., Richards, B. E., Wernert, P., Schreck, S., and Raffel, M., "Investigation of Three-Dimensional Dynamic Stall Using Computational Fluid Dynamics," *AIAA Journal*, Vol. 43, No. 5, 2005, pp. 1023–1033.

[10] Geissler, W., Dietz, G., and Mai, H., "Dynamic Stall on a Supercritical Airfoil," *Aerospace Science and Technology*, Vol. 9, No. 5, 2005, pp. 390–399. doi:10.1016/j.ast.2005.01.012

[11] Tan, C. M., and Carr, L. W., "The AFDD International Dynamic Stall Workshop on Correction of Dynamic Stall Models with 3-D Dynamic Stall Data," NASA TM 110375; also U.S. Army Aviation and Troop Command TR 96-A-009, July 1996.

[12] Petot, D., Arnaud, G., Stevens, J., Dieterich, O., van der Wall, B. G., Young, C., and Szechenyi, E., "Stall Effects and Blade Torsion: An Evaluation of Predictive Tools," *Journal of the American Helicopter Society*, Vol. 44, Oct. 1999, pp. 320–331.

[13] Johnson, W., "Rotorcraft Aerodynamics Models for a Comprehensive Analysis," *Proceedings of the 54th AHS Annual Forum*, AHS International, Alexandria, VA, May 1998.

[14] Leishman, J. G., and Beddoes, T. S., "A Semi-Empirical Model for Dynamic Stall," *Journal of the American Helicopter Society*, Vol. 34, July 1989, pp. 3–17.

[15] Wilby, P. G., "The Aerodynamic Characteristics of Some New RAE Blade Sections, and Their Potential Influence on Rotor Performance," *5th European Rotorcraft and Powered Lift Aircraft Forum*, *Vertica*, Vol. 4, No. 2, 1980, pp. 121–133.

[16] Galbraith, R. A. McD., and Leishman, J. G., "A Micro-Computer Based Test Facility for the Investigation of Dynamic Stall," International Conference on the Use of Micros in Fluid Engineering, British Hydromechanics Research Association, Paper E3, London, June 1983.

[17] Lober, P. F., and Carter, F. O., "Unsteady Stall Penetration Experiments at High Reynolds Number," United Technologies Research Center Rept. R87-956939-3, East Hartford, CT, 1987; also U.S. Air Force Office of Scientific Research TR-87-1202, Apr. 1987.

[18] Sheng, W., Galbraith, R. A. McD., and Coton, F. N., "A New Stall-Onset Criterion for Low Speed Dynamic-Stall," *Journal of Solar Energy Engineering*, Vol. 128, Nov. 2006, pp. 461–471. doi:10.1115/1.2346703

[19] Sheng, W., Galbraith, R. A. McD., and Coton, F. N., "Improved Dynamic-Stall-Onset Criterion at Low Mach Numbers," *Journal of Aircraft*, Vol. 44, No. 3, 2007, pp. 1049–1052.

[20] Beddoes, T. S., "A Synthesis of Unsteady Aerodynamic Effects Including Stall Hysteresis," *Vertica*, Vol. 1, No. 2, 1976, pp. 113–123.

[21] Beddoes, T. S., "Onset of Leading Edge Separation Effects Under Dynamic Conditions and Low Mach Number," *Proceedings of the 34th AHS Annual Forum*, AHS International, Alexandria, VA, May 1978.

[22] Beddoes, T. S., "Representation of Airfoil Behaviour," *Vertica*, Vol. 7, No. 2, 1983, pp. 183–197.

[23] Beddoes, T. S., "Practical Computation of Unsteady Lift," *Vertica*,

Vol. 8, No. 1, 1984, pp. 55–71.
[24] Niven, A. J., Galbraith, R. A. McD., and Herring, D. G. F., "Analysis of Reattachment During Ramp Down Tests," *Vertica*, Vol. 13, No. 2, 1989, pp. 187–196.
[25] Green, R. B., and Galbraith, R. A. McD., "Dynamic Recovery to Fully Attached Aerofoil Flow from Deep Stall," *AIAA Journal*, Vol. 33, No. 8, 1995, pp. 1433–1440.
[26] Green, R. B., and Galbraith, R. A. McD., "Phenomena Observed During Aerofoil Ramp-down Motions from the Fully Separated State," *The Aeronautical Journal*, Vol. 98, Nov. 1994, pp. 349–356.
[27] Ericsson, L. E., "Dynamic Airfoil Flow Separation and Reattachment," *Journal of Aircraft*, Vol. 32, No. 6, 1995, pp. 1191–1197.
[28] Ahmed, S., and Chandrasekhara, M. S., "Reattachment Studies of an Oscillating Airfoil Dynamic Stall Flowfield," *AIAA Journal*, Vol. 32, No. 5, 1994, pp. 1006–1012.
[29] Schreck, S. J., Faller, W. E., and Luttges, M. W., "Dynamic Reattachment on a Downward Pitching Finite Wing," *Journal of Aircraft*, Vol. 33, No. 2, 1996, pp. 279–285.
[30] Green, R. B., Galbraith, R. A. McD., Niven, A. J., "Measurements of the Dynamic Stall Vortex Convection Speed," *The Aeronautical Journal*, Vol. 96, No. 958, 1992, pp. 319–327.
[31] Evans, W. T., and Mort, K. W., "Analysis of Computed Flow Parameters for a Set of Sudden Stalls in Low Speed Two-Dimensional Flow," NACA TND-85, 1959.